Scale Up of Adsorption Column Experiments

M. Calvo-Schwarzwalder [1], A. Valverde [2], A Cabrera-Codony [3], M. Aguareles [4] and T.G. Myers [2,†],

[1] *Zayed University, Abu Dhabi, UAE*
[2] *Centre de Recerca Matemàtica, Bellaterra, Spain*
[3] *Laboratory of Chemical and Environmental Engineering (LEQUIA), Universitat de Girona, Girona, Spain*
[4] *Dept. d'Informàtica i Matemàtica Aplicada, Universitat de Girona, Girona, Spain*

(*Communicated to* MIIR *on 21 April 2023*)

Study Group: MISGSA 2022, University of the Witwatersrand, 7–11 February 2022

Communicated by: David P. Mason

Industrial Partner: Laboratory of Chemical and Environmental Engineering (LEQUIA), Universitat de Girona.

Presenter: Alba Cabrera-Codony, LEQUIA; Timothy G. Myers, Centre de Recerca Matemàtica.

Team Members: M. Aguareles, Universitat de Girona; M. Calvo-Schwarzwalder, Zayed University; T.G. Myers, Centre de Recerca Matemàtica; F.Z. Nouri, Université Badji Mokhtar-Annaba; A. Valverde, Centre de Recerca Matemàtica.

Industrial Sector: Environment

Key Words: Contaminant removal; Mathematical modelling; Fluid Dynamics; Adsorption.

MSC2020 Codes: 35Q35

† Corresponding Author: `tmyers@crm.cat`

Summary

Sorption columns are used to remove contaminants from a flowing fluid in a wide variety of industrial settings. To better understand the sorption process experiments are typically carried out in small columns, of the order 1cm × 15cm. Industrial sorption columns are of the order 1m × 5m. It is well-known that results from laboratory experiments do not scale-up well and so provide limited information to aid in the design of large equipment. In this report we analyse two standard sorption models, which agree well with data from small-scale experiments, and demonstrate that they cannot qualitatively match data from larger experiments. We then develop a simple mathematical model which extends the earlier work and permits the inclusion of size effects. This sets the scene for subsequent studies into the scale-up process.

1 Introduction

Perhaps the greatest danger currently facing mankind concerns environmental challenges and climate change. In the most recent IPCC (Intergovernmental Panel on Climate Change) report [IPCC2021] on climate change it is stated that "It is unequivocal that human influence has warmed the atmosphere, ocean and land. [...] Observed increases in well-mixed greenhouse gas concentrations since around 1750 are unequivocally caused by human activities". The link between climate change and human activity has been apparent for many years, it is therefore all the more tragic that first world countries could easily reduce emissions and achieve green energy targets. The well-known goal of maintaining the global temperature rise between 1.5-2°C can now only be achieved through drastic emission cuts combined with the active removal of greenhouse gases. To achieve even 2°C scenarios by 2050, almost 6 billion tonnes of CO_2 must be captured and stored each year. Similarly the UN Sustainable Goal of a "toxic free environment" requires the removal of a multitude of existing contaminants. The president of COP26, held in Glasgow in November 2021, stated that "We can now say with credibility that we have kept 1.5 degrees alive. But, its pulse is weak and it will only survive if we keep our promises and translate commitments into rapid action."

One practical method of removing fluid based environmental contaminants is column sorption, either through absorption or adsorption. Column sorption involves passing a fluid through a tube filled with a material capable of capturing certain components of the fluid. A standard laboratory experiment would involve a column of the order 20cm long and radius 5mm with a steady flow and contaminant escaping after around 15 minutes. Industrial columns are of the order 5m tall and may run continuously for months with a constantly varying gas intake. The environmental advantages of sorption processes are offset by an increase in cost, which makes the technology less attractive. Irlam [2] suggests that while CO_2 emissions from a power plant may typically be reduced by 90% there is an increase of between 45-70% in energy costs.

(a) (b)

Figure 1. (a) Experimental setup at LEQUIA laboratory. (b) Industrial system (reproduced from [9] under the Creative Commons Attribution-Share Alike 3.0 Unported license).

Whenever new systems or materials are investigated it is clear that testing will commence at the laboratory scale, to verify any proposed improvements. However, practical equipment must be much larger, as demonstrated by the two pictures shown in Fig. 1. A well-known problem arises when scaling up results from experimental studies to practical working devices. The aim of this study is to ascertain reasons for the failure to correctly scale the models.

A key quantity in any experimental study of sorption columns is the breakthrough curve, which represents the contaminant concentration at the outlet. This is an easily measurable quantity and there exists a large amount of breakthrough data in the literature. No new model will be trusted without verification against such data. In Fig. 2 we present two breakthrough curves reported by Liang *et al* [3] which show the ratio of the outlet concentration of phosphorous divided by the inlet value, c_0, after passing through a column filled with biochar microspheres (MBCQ) with typical dimension of 3 and 9mm. With the 3mm particles very little contaminant, approximately $0.04c_0$ escapes until approximately 100 minutes when it starts to increase, finally reaching the inlet value which indicates the adsorbent material is now full to capacity with phosphorous. The 9mm particle curve shows an approximately linear increase in concentration for approximately 120 minutes before subsequently taking the same form as the 3mm curve.

In Fig. 3 we present two different sets of breakthrough curves for toluene adsorption on Norit RB3 charcoal. The data comes from the work of the LEQUIA group and is discussed in more detail in [7]. In the first figure the typical particle dimension for the two experiments is 0.15-0.212mm and 0.425-0.6mm, the flow rate is 205mL/min. In the second figure and additional particle size 0.212-0.425mm is shown while the flow rate has increased to 260mL/min. Fig. 3a) shows what may be considered a "standard" form for the experimental breakthrough curves: the outlet concentration is zero for a significant period of time followed by an elongated S-shaped symmetric curve. Fig. 3b) also shows an initial period with no breakthrough but the two curves for the larger particles appear to have lost the S-shape. For the 0.425-0.6mm adsorbent there appears to be two almost linear sections.

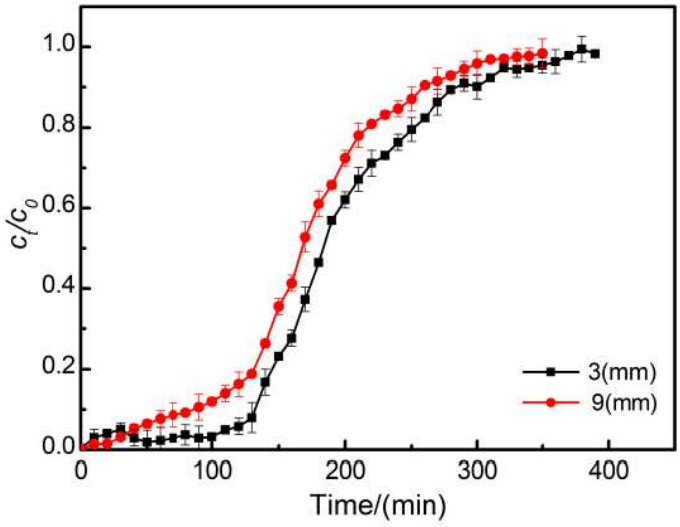

Figure 2. Experimental breakthrough curves for two pellet dimensions. Reproduced from Fig. 4 [3] under Creative Commons License V.4

In each set of experiments other operational parameters are kept fixed. Liang *et al* [3] state that in their experiments there occurs significant chemisorption while the toluene adsorption has been shown in previous works to agree well with Langmuir adsorption kinetics with physisorption as controlling mechanism. Despite the significant differences in their adsorption kinetics, the effect of particle size in both is similar. A reasonable interpretation is then that some other effect becomes significant with the larger particles. A possible mechanism is intra-particle diffusion, which should be fast with small particles but slower with large ones such that for sufficiently large particles the intra-particle diffusion time-scale becomes of the same order as adsorption. We will investigate this later.

In the following sections we will investigate existing models coupling mass flow to a mass sink equation, to see if they can be adapted in a simple manner to deal with the system changes on scale-up. In the final section we investigate a more complex model which incorporates intra-particle diffusion.

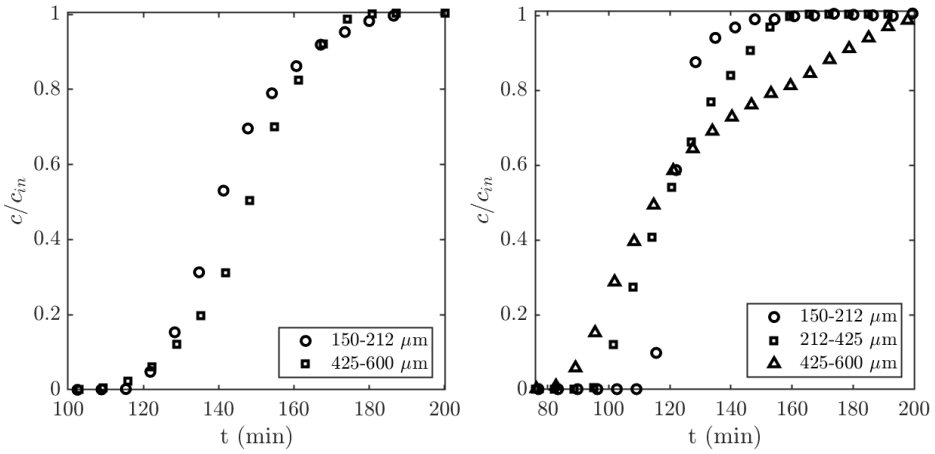

Figure 3. (a) Toluene adsorption experimental data at 205 mL/min. (b) Toluene adsorption experimental data at 260 mL/min.

2 Derivation of averaged advection-diffusion equation

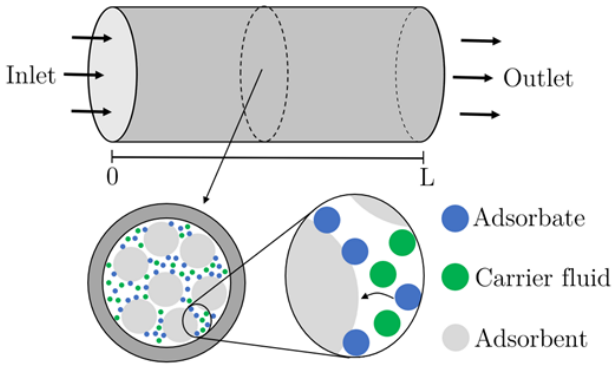

Figure 4. Schematic of the experimental setup.

Fig. 4 shows the set-up for the mathematical model, fluid flows through a circular cross-section pipe and contaminant particles attach to the surface of the adsorbate. Due to the random packing of the adsorbent material we expect that, on average, the flow will be radially symmetric, which allows us to write the mass balance

$$\frac{\partial c}{\partial t} + \frac{\partial}{\partial z}(uc) = D\left[\frac{\partial^2 c}{\partial z^2} + \frac{1}{r}\frac{\partial}{\partial r}\left(r\frac{\partial c}{\partial r}\right)\right], \tag{2.1}$$

where c is the concentration of contaminant [kg/m^3], u the interstitial velocity and D the diffusion coefficient. Due to the complex nature of the fluid flow u is generally taken to be constant. An alternative approach is to describe the fluid velocity via the Darcy-Brinkman approach, see Mondal *et al* [4]. With this model the effect of the column walls may be accounted for. The thickness of the wall boundary layer is quantified by the Darcy number. Using parameter values appropriate for column sorption we obtained a value of

the order of 10^{-4}, indicating the presence of a very thin boundary layer. In the study of [4] the Darcy number was of order 10^{-7}. Consequently it is reasonable to assume the velocity is constant throughout the cross-section.

Equation (2.1) holds within the fluid, for this reason there is no sink term, since mass loss occurs at the solid-fluid boundaries. The sink term enters the flow equation only when we average over a cross-section, which then incorporates both solid and liquid regions. So, we now define an average concentration over a typical cross-section

$$\phi\pi R^2\bar{c} = 2\pi\int_0^R crdr\,, \tag{2.2}$$

where ϕ represents the void fraction (that is, the space occupied by the fluid). Then, integrating Eq. (2.1) gives

$$\frac{\phi R^2}{2}\left[\frac{\partial\bar{c}}{\partial t} + u\frac{\partial\bar{c}}{\partial z} - D\frac{\partial^2\bar{c}}{\partial z^2}\right] = D\int_0^R \frac{\partial}{\partial r}\left(r\frac{\partial c}{\partial r}\right)dr\,. \tag{2.3}$$

Once evaluated, the final integral involves $D\,(\partial c/\partial r)$ terms. Since the equation only holds in the void region the integral must be split accordingly

$$D\int_0^R \frac{\partial}{\partial r}\left(r\frac{\partial c}{\partial r}\right)dr = D\,R\,\frac{\partial c}{\partial r}\bigg|_{r=R} + D\sum_{\text{internal}} r_i\frac{\partial c_i}{\partial r}\,. \tag{2.4}$$

Since there is no flux into the column wall the first term on the right hand side vanishes while the summation of fluxes at the internal boundaries equates to the mass sink. If mass loss occurs over the solid fraction we may express this as

$$D\sum_{\text{internal}} r_i\frac{\partial c_i}{\partial r} = (1-\phi)\frac{R^2}{2}\rho_p\frac{\partial\bar{q}}{\partial t}\,, \tag{2.5}$$

where ρ_p is the density of the adsorbent (as opposed to the material adsorbed). This is the appropriate density provided we take the standard definition from the chemistry literature that $\bar{q}$ is the mass of adsorbate divided by the (initial) mass of adsorbent, measured in [kg/kg]. The mass balance for the contaminant is now

$$\frac{\partial\bar{c}}{\partial t} + u\frac{\partial\bar{c}}{\partial z} = D\frac{\partial^2\bar{c}}{\partial z^2} - \frac{(1-\phi)}{\phi}\rho_p\frac{\partial\bar{q}}{\partial t}\,. \tag{2.6}$$

In §4 we will work with a slightly modified version which accounts for the porosity inside the particles. A simple calculation determines the final amount of material adsorbed during the process $\bar{q}_e = (M_f - M_i)/M_i$. This is used to determine isotherm graphs (plots of $\bar{q}_e$ against the equilibrium concentration $\bar{c}_e$).

2.1 Mass sink models

The classic adsorption sink model is the Langmuir equation

$$\frac{\partial\bar{q}}{\partial t} = k_a\bar{c}\,(\bar{q}_m - \bar{q}) - k_d\bar{q}\,, \tag{2.7}$$

where k_a, k_d represent the adsorption and desorption coefficients and $\bar{q}_m$ is the maximum possible value of $\bar{q}$. However, note that the k's do not have the same units, the ratio

k_d/k_a has the units of a concentration. If we set $\partial\bar{q}/\partial t = 0$ we find the isotherm $\bar{q}_e = \bar{c}_e\bar{q}_m/(\bar{c}_e + k_d/k_a)$, where the subscript e denotes equilibrium. Plots of experimental data for $1/\bar{q}_e$ versus $1/\bar{c}_e$ permits the calculation of $\bar{q}_m$ and the ratio k_a/k_d. In a static experiment $\bar{c}_e$ is measured after a sufficiently long time such that adsorption has ended. In a column experiment $\bar{c}_e = \bar{c}_{\text{in}}$ is the inlet velocity.

Given the non-linear nature of Eq. (2.7), a linearised version is often used

$$\frac{\partial\bar{q}}{\partial t} = k_l(\bar{q}_e - \bar{q})\,. \tag{2.8}$$

This approximates the Langmuir form but requires a non-vanishing contaminant concentration. If $\bar{c} \to 0$, such as ahead of the contaminant wave, Langmuir indicates either zero adsorption or desorption (if $\bar{q} \neq 0$). Whereas if $\bar{c} = \bar{q} = 0$ the linear form suggests adsorption is at its highest rate, despite there being no contaminant to adsorb. This commonly used form should be applied with care.

2.2 Boundary conditions

Appropriate boundary and initial conditions for this system are

$$u_i\bar{c}(0,t) - D\left.\frac{\partial\bar{c}}{\partial z}\right|_{z=0} = Q_i\,, \tag{2.9a}$$

$$\left.\frac{\partial\bar{c}}{\partial z}\right|_{z=L} = 0\,, \tag{2.9b}$$

$$\bar{c}(z,0) = \bar{q}(z,0) = 0\,. \tag{2.9c}$$

The first condition is a balance between the known, incoming contaminant flux Q_i and the flux just inside the column. The contaminant flux is determined through the total fluid flux: if the total flux is Q then the velocity just at the column inlet is $u_{i0} = Q/(\phi\pi R^2)$ then $Q_i = u_{i0}c_{\text{in}}$, where c_{in} is the contaminant concentration in the incoming fluid. When only trace amounts of contaminant are removed then the velocity is constant throughout the column and the initial interstitial velocity $u_{i0} = u_i$ is constant. At the outlet continuity of flux would balance two expressions of the form $u\bar{c} - D(\partial\bar{c}/\partial z)$. Inside the column this is identical to the expression provided in Eq. (2.9a), but applied at $z = L$, just outside the column, since the fluid is not transported away we expect the velocities match across the exit. Assuming the concentration just outside the column matches that just inside and the external diffusion is small (inside the column D is determined by the flow around the porous material, outside it is standard Brownian diffusion which is orders of magnitude smaller, hence $D_a \ll D$), we obtain Eq. (2.9b).

If all the contaminant is adsorbed within the column, the condition at $z = L$ may not be appropriate. All the curves presented in Fig. 3 show an outlet concentration of zero until 80 to 100 minutes. This indicates that during the initial period the contaminant was fully adsorbed before reaching the column outlet. Assuming a moving front, located at $z = s(t)$, we may replace Eq. (2.9b) with

$$\bar{c}(s(t),t) = \left.\frac{\partial\bar{c}}{\partial z}\right|_{z=s(t)} = 0\,. \tag{2.10}$$

The latter condition is a consequence of zero contaminant flux at the front, that is,

$\bar{c} - D(\partial\bar{c}/\partial z) = 0$ at $z = s(t)$. The single condition at $z = L$ has been replaced by two at $z = s(t)$ since the position $s(t)$, which defines the domain, is unknown.

2.3 Non-dimensional Formulation

We scale the variable as follows:

$$\bar{c} \to c_{\text{in}}\hat{c}\,, \qquad \bar{q} \to \bar{q}_m\hat{q}\,, \qquad z \to \mathcal{L}\hat{z}\,, \qquad t \to \tau\hat{t}\,. \tag{2.11}$$

Upon defining the length scale as $\mathcal{L} = uc_{\text{in}}\tau\phi/((1-\phi)\rho_p\bar{q}_m)$, which balances the advection and sink terms, the mass balance in Eq. (2.6) becomes

$$\text{Da}\frac{\partial\hat{c}}{\partial\hat{t}} + \frac{\partial\hat{c}}{\partial\hat{z}} \quad = \quad \text{Pe}^{-1}\frac{\partial^2\hat{c}}{\partial\hat{z}^2} - \frac{\partial\hat{q}}{\partial\hat{t}}\,, \tag{2.12}$$

where $\text{Da} = \mathcal{L}/u\tau$ is the Damköhler number and $\text{Pe}^{-1} = D/(u\mathcal{L})$ is the inverse Péclet number and both parameters are typically considered to be small [7].

The time scale is chosen to balance the mass sink equations. If we consider the linear form of Eq. (2.8), we choose $\tau = 1/k_l$, which leads to

$$\frac{\partial\hat{q}}{\partial\hat{t}} = \hat{q}_e - \hat{q}\,, \tag{2.13a}$$

whereas when considering the Langmuir equation (2.7) we choose $\tau = 1/(k_a c_{\text{in}})$ to find

$$\frac{\partial\hat{q}}{\partial\hat{t}} = \hat{c}\,(1-\hat{q}) - k\hat{q}\,. \tag{2.13b}$$

In Eq. (2.13a), $\hat{q}_e = \bar{q}_e/\bar{q}_m = 1/(1+k)$ and in Eq. (2.13b), $k = k_d/k_a c_{\text{in}}$.

The non-dimensional boundary conditions are

$$\hat{c}\,(0,\hat{t}) - \text{Pe}^{-1}\frac{\partial\hat{c}}{\partial\hat{z}}\bigg|_{\hat{z}=0} = 1\,, \tag{2.14a}$$

$$\frac{\partial\hat{c}}{\partial\hat{z}}\bigg|_{\hat{z}=\hat{L}} = 0\,, \tag{2.14b}$$

$$\hat{c}(\hat{z},0) = \hat{q}(\hat{z},0) = 0\,, \tag{2.14c}$$

where $\hat{L} = L/\mathcal{L}$. In the case of a moving front we substitute Eq. (2.14b) by

$$\hat{c}\,(\hat{s},\hat{t}) = \frac{\partial\hat{c}}{\partial\hat{z}}\bigg|_{\hat{z}=\hat{s}} = 0\,, \tag{2.15}$$

where $\hat{s} = s/\mathcal{L}$.

The above system is standard in the literature however mathematical analyses of the equations are rare. A number of solutions focussed on the breakthrough curve are based on *ad hoc* assumptions regarding the probability of contaminant escaping at the outlet, the exception being [5, 6] which use a travelling wave substitution to capture the behaviour throughout the column beyond the initial transient. In the following we will take the travelling wave approach and focus on breakthrough data. The travelling wave is well-designed for this, since although it is inaccurate for small times by the time breakthrough is achieved the errors are negligible.

3 Travelling wave solutions

In this section we apply the travelling wave approach to the non-dimensional problem defined in §2.3, focussing first on the linear mass sink equation and secondly on the non-linear Langmuir equation.

3.1 Linear mass sink

Consider the system defined by equations (2.12, 2.13a). We define the travelling wave co-ordinate $\eta = \hat{z} - \hat{s}\left(\hat{t}\right)$ where $\mathrm{d}\hat{s}/\mathrm{d}\hat{t} = \hat{v}$ and $\hat{c}\left(\hat{z},\hat{t}\right) = C(\eta)$, $\hat{q}\left(\hat{z},\hat{t}\right) = Q(\eta)$, which leads to

$$-\hat{v}\mathrm{Da}C_\eta + C_\eta = \mathrm{Pe}^{-1}C_{\eta\eta} + \hat{v}Q_\eta\,, \tag{3.1a}$$

$$-\hat{v}Q_\eta = \hat{q}_e - Q\,. \tag{3.1b}$$

where the derivatives with respect to η are written as subscripts for simplicity. In this approach we consider the boundary conditions at the moving front rather than at $\hat{z} = \hat{L}$, which leads to

$$C(0) = C_\eta(0) = 0\,. \tag{3.2a}$$

Adsorption requires contaminant, so it must reach zero at the contaminant front

$$Q(0) = 0\,. \tag{3.2b}$$

In the travelling wave form we cannot apply conditions at $\hat{z} = 0$ and instead assume the solution only holds when $\hat{s}\left(\hat{t}\right)$ is sufficiently large such that we may write $\eta|_{\hat{z}=0} = -\hat{s}\left(\hat{t}\right) \to -\infty$. As we will see later the solution has an exponential dependence on $-\hat{s}\left(\hat{t}\right)$ and so errors rapidly decay, so justifying this approximation. In the far-field the travelling wave will require the adsorbent to be in its equilibrium state and the concentration to be at the inlet value (in line with the equilibrium isotherm), hence

$$\lim_{\eta\to-\infty} C = 1\,, \qquad \lim_{\eta\to-\infty} Q = \hat{q}_e\,. \tag{3.3}$$

The first condition is consistent with extending the $z = 0$ condition back to $-\infty$, such that the gradient tends to zero.

Inspection of the above system should immediately suggest this cannot account for size variation. The system only contains two parameters, both of which are small and hence unlikely to affect the solution form. The particle size could affect the void fraction, ϕ, and consequently the interstitial velocity. Since the Damköhler number is small, these would then mainly affect the length-scale $\mathcal{L}$ and hence the horizontal scale of the solutions. This form has previously been shown to match data for small particles, of the order μm, with an initial sharp rise in outlet concentration [5]. A change in the length-scale cannot account for the initial linear form exhibited by the 9mm particle data of Fig. 2.

Henceforth we will set $\mathrm{Pe}^{-1} = 0$, since its only real effect is to slightly alter the shape of the breakthrough curve in the immediate vicinity of the moving front. Even retaining this term the governing equations may be solved, but the final form is clearer without it. Although Da is also small we retain it since it has no effect on the calculations. Integrating

equation (3.1a) and applying the conditions at $\eta = 0$ results in

$$C(\eta) = \frac{\hat{v}}{1 - \hat{v}\mathrm{Da}} Q(\eta)\,. \tag{3.4}$$

Applying the far-field conditions determines the velocity $\hat{v} = (\hat{q}_e + \mathrm{Da})^{-1}$. Integrating Eq. (3.1b) yields

$$C(\eta) = 1 - \exp\left(\frac{\eta}{\hat{v}}\right), \qquad Q(\eta) = \hat{q}_e\left[1 - \exp\left(\frac{\eta}{\hat{v}}\right)\right]. \tag{3.5}$$

To revert back to the (z,t) system requires an expression for $\hat{s}\left(\hat{t}\right)$. Given that $\mathrm{d}\hat{s}/\mathrm{d}\hat{t} = \hat{v}$, where $\hat{v}$ is known, we may write $\hat{s}\left(\hat{t}\right) = \hat{v}\hat{t} + \hat{s}_0$ where $\hat{s}_0$ is unknown and cannot be determined from the initial condition since this is where the travelling wave does not hold. Instead we will take information from the breakthrough curve, to do this we revert to the dimensional co-ordinates and write

$$\frac{c(z,t)}{c_{\mathrm{in}}} \quad = \quad 1 - \exp\left(\frac{z - s_0}{\tau v} - \frac{t}{\tau}\right), \tag{3.6}$$

where the dimensional speed of the wave is

$$v = \frac{\mathcal{L}\hat{v}}{\tau} = \frac{u}{1 + (1-\phi)\rho_p q_e/(\phi c_{\mathrm{in}})}\,. \tag{3.7}$$

From the experimental data we may determine the time $t_{1/2}$ when the concentration reaches half the inlet value and then, upon substituting $\tau = 1/k_l$,

$$\frac{c(z,t)}{c_{\mathrm{in}}} = 1 - \frac{1}{2}\exp\left[k_l\frac{z-L}{v} - k_l\left(t - t_{1/2}\right)\right], \tag{3.8}$$

and the breakthrough curve is

$$\frac{c(L,t)}{c_{\mathrm{in}}} = 1 - \frac{1}{2}\exp\left(k_l(t_{1/2} - t)\right) = \frac{q(L,t)}{q_e}\,. \tag{3.9}$$

This form for the breakthrough curve shows no dependence on the particle size or void fraction. The time $t_{1/2}$ will be affected by the void fraction (for a given pressure drop across the column) but this will only determine the position of the curve, not it's shape. Further, if we focus on the gradient

$$\left.\frac{dc}{dt}\right|_{z=L} = \frac{k_l c_{\mathrm{in}}}{2}\exp\left(k_l(t_{1/2} - t)\right), \tag{3.10}$$

then it is apparent that for small $t < t_{1/2}$ the concentration does not exhibit linear growth.

3.2 Nonlinear sink model

A similar analysis as in §3.1 can be performed when considering Eqs. (2.12, 2.13b). In this case, the resulting dimensional expressions for the concentration and adsorbed material are

$$\frac{c(z,t)}{c_{\mathrm{in}}} = \frac{1}{1 + \exp\left[k_a c_{\mathrm{in}}((x-L)/v + (t_{1/2} - t))\right]} = \left(1 + \frac{k_d}{k_a c_{\mathrm{in}}}\right)\frac{q(z,t)}{q_m}, \tag{3.11}$$

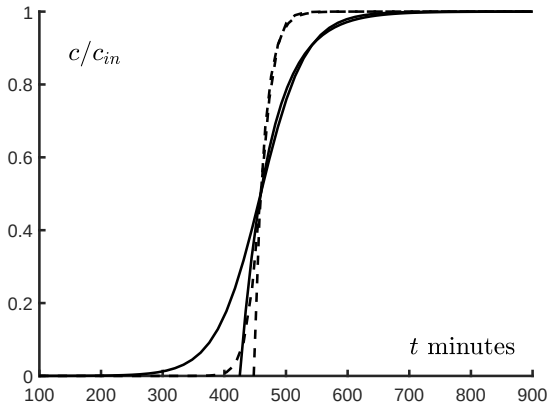

Figure 5. Breakthrough curves predicted by equations (3.9, 3.13a), solid lines come from taking the experimentally determined k_a value, dashed lines with three times this value. The curves with zero gradient at first breakthrough correspond to (3.13a).

where the velocity of the wave front is now

$$v = \frac{u}{1 + (1-\phi)\rho_p q_m/(\phi c_{\text{in}}(1+k))}\,. \tag{3.12}$$

In the limit $k_d \to 0$ this matches the velocity from the linear adsorption model.

At the outlet, the breakthrough equations are

$$c(L,t) = \frac{c_{\text{in}}}{1 + \exp(k_a c_{\text{in}}(t_{1/2} - t))}\,, \tag{3.13a}$$

$$q(L,t) = \frac{q_m k_a c_{\text{in}}}{(k_a c_{\text{in}} + k_d)(1 + \exp(k_a c_{\text{in}}(t_{1/2} - t))}\,. \tag{3.13b}$$

An interesting feature of this solution is that the shape of the breakthrough curve, $c(L,t)$, provides no information on the desorption although the velocity, which is indicative of how soon breakthrough first occurs, does depend on the ratio of desorption to adsorption.

In Fig. 5 we present breakthrough curves corresponding to an experimental study of toluene removal [7]. Parameter values are taken from that study: for the case $c_{\text{in}} = 4.1 \times 10^{-4}\text{kg/m}^3$ the adsorption coefficients found were to be $k_l = 3.4 \times 10^{-4}\text{s}^{-1}$, $k_a = 1.2\text{m}^3/(\text{kg s})$ and $t_{1/2} = 459$ minutes. The solid lines represent the breakthrough curves of equations (3.9, 3.13a) (the one with a zero initial gradient is (3.13a)). To demonstrate the effect of changing parameter values the dashed lines show results with $k_a \to 3k_a$ (whilst keeping $t_{1/2}$ fixed). Since, for a given flow, the adsorption coefficient is the only parameter which can affect the solution it is clear that this cannot significantly affect scaling up. Consequently, in the following section we add an extra level of complexity.

4 Intra-particle diffusion model

As the size of the adsorbing material increases, it is reasonable to assume that diffusion into these particles may affect the overall adsorption process. Therefore in this section we consider an additional effect, which is the concentration of contaminant inside the particle. To distinguish from previous quantities we will use the subscript i to denote interior. For simplicity, we assume that the particles are all spherical with internal porosity ϕ_i and radius R_i. By assuming spherical symmetry we must only consider one additional local variable $0 < r_i \leq R_i$.

Assuming that the flow inside the particles is driven by diffusion we may analyse the concentration within the particles gaps through a standard diffusion equation

$$\frac{\partial c_i}{\partial t} = \frac{D_i}{r_i^2}\frac{\partial}{\partial r_i}\left(r_i^2 \frac{\partial c_i}{\partial r_i}\right), \tag{4.1}$$

where D_i is the diffusivity inside the particles. This equation holds over the void area within the particle. We define an average particle concentration

$$\phi_i \frac{4}{3}\pi R_i^3 \bar{c}_i = \int_0^{R_i} 4\pi r_i^2 c_i \, dr \,. \tag{4.2}$$

Applying this to the diffusion equation

$$\begin{aligned} \phi_i \frac{4}{3}\pi R_i^3 \frac{\partial \bar{c}_i}{\partial t} &= 4\pi D_i \left[R_i^2 \frac{\partial c_i}{\partial r_i}\bigg|_{r_i = R_i} + \sum_{\text{internal}} r_i^2 \frac{\partial c_i}{\partial r_i} \right] \\ &= 4\pi R_i^2 k_i (\bar{c} - \bar{c}_i) + 4\pi D_i \sum_{\text{internal}} r_i^2 \frac{\partial c_i}{\partial r_i} \,, \end{aligned} \tag{4.3}$$

where we have approximated the flux at $r_i = R_i$ by a linear kinetic relation

$$D_i \frac{\partial c_i}{\partial r_i} = k_i (\bar{c} - \bar{c}_i) \,, \tag{4.4}$$

for some mass transfer coefficient k_i (measured in [m/s]). The sum of fluxes within the particle equates to the total adsorption onto the solid hence

$$\phi_i \frac{4}{3}\pi R_i^3 \frac{\partial \bar{c}_i}{\partial t} = 4\pi R_i^2 k_i (\bar{c} - \bar{c}_i) - (1 - \phi_i)\frac{4}{3}\pi R_i^3 \rho_i \frac{\partial \bar{q}_i}{\partial t} \,. \tag{4.5}$$

Note, we distinguish between the mass sink within the particle $\bar{q}_i$ and that within the flow $\bar{q}$. The former is an average over a single particle with a void fraction ϕ_i the latter an average over the column cross-section with a void fraction ϕ. We define an adsorbate density, ρ_i, through the adsorbent volume within the particle as opposed to the previous density defined over the total particle volume within the column such that $\rho_p = (1-\phi_i)\rho_i$.

The internal mass balance finally reduces to

$$\frac{\partial \bar{c}_i}{\partial t} = \frac{3k_i}{\phi_i R_i}(\bar{c} - \bar{c}_i) - \frac{(1 - \phi_i)}{\phi_i}\rho_i \frac{\partial \bar{q}_i}{\partial t} \,, \tag{4.6}$$

which is subject to

$$\bar{c}_i(z, t_s) = \bar{q}_i(z, t_s) = 0 \,. \tag{4.7}$$

This condition is a statement that the concentration and hence amount adsorbed within

the particle is zero until the front reaches there, at time $t_s(z)$. Since $\bar{c} = \bar{c}(z,t)$ then both $\bar{c}_i, \bar{q}_i$ depend on z, t. The coefficient k_i reflects how contaminant attaches to or enters the surface of the adsorbent particle. It must account for the fact that the surface has gaps and differs from the adsorption and desorption coefficients for attachment within the particle. It must be determined by matching with experiments.

The correct kinetic relation should in fact involve $(c - c_i)|_{r_i = R_i}$ but since we now use average values this must be approximated by $(\bar{c} - \bar{c}_i)$ (which will then affect the value of k_i). Equation (4.6) therefore states that the contaminant concentration within the particle decreases due to removal by adsorption over the solid region and increases due to the input of new contaminant at the outer boundary.

To relate the adsorption rates between the present model and that neglecting intra-particle diffusion, we note that the rate of mass adsorption in the latter must balance the rate at which mass increases inside the particle, either in the fluid or as adsorbate,

$$\rho_p \frac{\partial \bar{q}}{\partial t} = \phi_i \frac{\partial \bar{c}_i}{\partial t} + (1 - \phi_i)\rho_i \frac{\partial \bar{q}_i}{\partial t} = \frac{3k_i(\bar{c} - \bar{c}_i)}{R_i} \,. \tag{4.8}$$

The final equality follows directly from equation (4.6). Replacing $\rho_p \bar{q}_t$ in equation (2.6) leads to

$$\frac{\partial \bar{c}}{\partial t} + u\frac{\partial \bar{c}}{\partial z} = D\frac{\partial^2 \bar{c}}{\partial z^2} - \frac{3k_i(1-\phi)}{\phi R_i}(\bar{c} - \bar{c}_i) \tag{4.9}$$

$$= D\frac{\partial^2 \bar{c}}{\partial z^2} - \frac{(1-\phi)}{\phi}\left[\phi_i \frac{\partial \bar{c}_i}{\partial t} + \rho_p \frac{\partial \bar{q}_i}{\partial t}\right] . \tag{4.10}$$

Writing the *shape factor* as $\xi = 3(1-\phi)/R_i$ we see that (4.9) reproduces the formula for randomly packed spherical particles, see [4, 8] for example.

The mass sink terms must be slightly modified to reflect the fact that adsorption occurs within the particle

$$\frac{\partial \bar{q}_i}{\partial t} = k_l(\bar{q}_e - \bar{q}_i) \,, \tag{4.11a}$$

$$\frac{\partial \bar{q}_i}{\partial t} = k_a \bar{c}_i(\bar{q}_m - \bar{q}_i) - k_d \bar{q}_i \,. \tag{4.11b}$$

This change does not affect the isotherm, which requires $\bar{c}_i = c_{\text{in}}$ at equilibrium.

4.1 Non-dimensional Formulation

Focusing on the data shown in Fig. 2 it appears that adsorption from larger particles affects the early breakthrough but then the curve resembles those of smaller particles. The close resemblance of results suggests that the previous scaling remains appropriate in this case, however we note that shifting to the industrial scale may require consideration of a different time-scale.

Since the concentration within the particle is due to contaminant entering with the flow we scale $\bar{c}_i$ with c_{in} to find

$$\text{Da}\frac{\partial \hat{c}}{\partial \hat{t}} + \frac{\partial \hat{c}}{\partial \hat{z}} = \text{Pe}^{-1}\frac{\partial^2 \hat{c}}{\partial \hat{z}^2} - \alpha\frac{\partial \hat{c}_i}{\partial \hat{t}} - \frac{\partial \hat{q}_i}{\partial \hat{t}} \,, \tag{4.12}$$

where $\alpha = \phi_i c_{\text{in}}/(\rho_p \bar{q}_m)$. Within the particle,

$$\beta(\hat{c} - \hat{c}_i) = \alpha \frac{\partial \hat{c}_i}{\partial \hat{t}} + \frac{\partial \hat{q}_i}{\partial \hat{t}}\,, \tag{4.13}$$

where $\beta = 3k_i c_{in}\tau/\rho_p \bar{q}_m R_i$.

The sink terms are now

$$\frac{\partial \hat{q}_i}{\partial \hat{t}} = \hat{q}_e - \hat{q}_i\,, \tag{4.14a}$$

$$\frac{\partial \hat{q}_i}{\partial \hat{t}} = \hat{c}_i(1 - \hat{q}_i) - k\hat{q}_i\,, \tag{4.14b}$$

and the boundary conditions are

$$\hat{c}_i(\hat{z}, \hat{t}_s) = \hat{q}_i(\hat{z}, \hat{t}_s) = 0\,. \tag{4.15}$$

4.2 Understanding the new parameters

In this new formulation, two additional parameters arise,

$$\alpha = \frac{\phi_i c_{\text{in}}}{\rho_p \bar{q}_m} = \text{Da}\frac{\phi_i(1-\phi)}{\phi}\,, \qquad \beta = \frac{3k_i c_{\text{in}}\tau}{\rho_p \bar{q}_m R_i} = \frac{\tau}{\tau_q}\,. \tag{4.16}$$

The first parameter is the ratio of maximum amount of contaminant that can occupy the particle, $\phi_i c_{\text{in}}$, to the maximum amount that can be adsorbed into the solid phase, $\rho_p \bar{q}_m = (1-\phi_i)\rho_i \bar{q}_m$. It can therefore be interpreted as an intrinsic parameter of the material, that is, depending on its physical and chemical properties but not on its size. A different interpretation can be defined in terms of the Damköhler number (Da), and the bed and particle porosity. In this sense, the parameter α is the equivalent Damköhler number but inside a particle (4.13). This is related to the fluid Damköhler number through the particle void and flow void and solid fractions. Since these quantities are usually between 0.1 and 1, the magnitude of the parameter α is typically of the same magnitude as Da.

For a better understanding of the second parameter it is worth noting that the problem now has an additional time scale. Balancing the adsorption term, $\partial \bar{q}_i/\partial t$ with the incoming contaminant term, $(\bar{c} - \bar{c}_i)$, determines $\tau_q = (\rho_p \bar{q}_m R_i)/3k_i c_{\text{in}}$. This represents the time-scale for contaminant entering at the particle boundary to be adsorbed by the solid. The parameter $\beta = \tau/\tau_q$ therefore represents the ratio of the reaction time-scale τ to the particle adsorption time-scale and may be considered a form of Thiele modulus. For sufficiently large R_i it may be sensible to work on the time-scale τ_q rather than τ.

4.3 Thoughts/Reduction to previous model as $R_i \to 0$

Given the prevalence of models such as those described in §2 as well as their success in capturing a wide variety of data it is desirable to demonstrate that the intra-particle diffusion model reduces to previous models in the appropriate limit.

The key parameters introduced in the new model are the particle void fraction and radius, ϕ_i, R_i. We anticipate that as these become small in some limit the previous models will appear. To avoid confusion we point out that adsorbents are typically porous materials, since this can maximize the surface available for adsorption. Consequently

the void fraction of the particles, ϕ_i, does not physically tend to zero. However, this doesn't mean that intra-particle diffusion always occurs. This relies on the relative size of the contaminant molecules and the adsorbent pores, e.g. macropores ($d_{pore} > 50$ nm), mesopores (2 nm $< d_{pore} <$ 50 nm) and micropores ($d_{pore} < 2$ nm). Intra-particle diffusion is only possible if the shortest dimension of the molecule is less than the pore size and, if it does occur, how significant is the diffusion through the range of pore sizes inside? This issue is considered in Cabrera-Codony *et al* [1] who report an exhaustive assessment of the dimensions of different siloxanes and the pore distribution of diverse activated carbons. If the smallest dimension of the contaminant molecules is greater than the pore diameter then the intra-particle diffusion model will not hold. This discussion suggests that taking the limit $\phi_i \to 0$ is not enough to move between the different forms of behaviour. A small particle of material with $\phi_i \approx 0$ would behave in the same manner as a large particle.

Now consider the variation of R_i, which affects the value of β: $\beta \to \infty$ as $R_i \to 0$ and $\beta \to 0$ as $R_i \to \infty$. In the limit $\beta \to \infty$ we observe that equation (4.13) reduces to $\hat{c} = \hat{c}_i$ and we may remove $\hat{c}_i$ from the system, however $\hat{q}_i$ remains. If we consider the non-dimensional form of the left hand terms of (4.8) we obtain $\hat{q}_t = \alpha \hat{c}_{it} + \hat{q}_{it}$. In the limit $\phi_i \to 0$ or Da $\to 0$ we find $\alpha \to 0$ and so $\hat{q} \to \hat{q}_i$ and we obtain an equivalence between the adsorbed mass expressions. The leading order system may now be written

$$\mathrm{Da}\frac{\partial \hat{c}}{\partial \hat{t}} + \frac{\partial \hat{c}}{\partial \hat{z}} = \mathrm{Pe}^{-1}\frac{\partial^2 \hat{c}}{\partial \hat{z}^2} - \frac{\partial \hat{q}}{\partial \hat{t}}\,, \tag{4.17a}$$

$$\hat{c}_i = \hat{c}\,, \tag{4.17b}$$

$$\frac{\partial \hat{q}}{\partial \hat{t}} = \hat{c}(1-\hat{q}) - k\hat{q}\,, \tag{4.17c}$$

and the standard model neglecting intra-particle diffusion is retrieved. To be clear we state that the reduction to the standard two equation system occurs for small R_i and ϕ_i.

5 Conclusions/Future Work

Experimental data for large and small columns, using large and small sorbent particles, exhibit a different form at early times. With large pellets an initial linear increase in the outlet concentration is observed, which then joins up to the exponential form typical of small pellet results. Standard models do not capture this linear behaviour, hence the goal of this meeting was to develop a suitable model which explains this early time growth.

To understand the sorption process we first investigated two standard models, developed for small column experiments. These accounted for the contaminant concentration in the fluid and an averaged mass sink in the sorbent material. In both cases there was little scope to include size effects. Returning non-dimensional to dimensional forms could only scale the solutions: there was no possibility of qualitative changes in the form. The inability to capture the initial linear concentration growth observed in experiments was confirmed through travelling wave solutions of the two models.

To include a new level of complexity we then developed a model which accounted for diffusion within the sorbent. This built on two earlier models taken from the literature but without the need to introduce the shape factor employed in these works. The re-

sulting system includes a term which accounts for the particle size and introduces a new time-scale. The new time-scale in particular could account for the change in early time behaviour when small and large particles are employed. During the meeting there was not enough time to analyse this model but studies are currently under way to produce numerical and approximate analytical results.

References

[1] A. Cabrera-Codony, E. Santos-Clotas, C.O. Ania, M.J. Martín. 2018. Competitive siloxane adsorption in multicomponent gas streams for biogas upgrading. *Chemical Engineering Journal*, **344**, 565–573.

[2] L. Irlam. 2017. Global costs of carbon capture and storage. *Global CCS Institute*, **16**.

[3] Q. Liang, X. Fu, P. Wang, X. Li and P. Zheng. 2022. Dynamic Adsorption Characteristics of Phosphorus Using MBCQ. *Water*, **14**, 508.

[4] R. Mondal, S. Mondal, K.V. Kurada, S. Bhattacharjee, S. Sengupta, M. Mondal, S. Karmakar, S. De and I.M. Griffiths. 2019. Modelling the transport and adsorption dynamics of arsenic in a soil bed filter. *Chemical Engineering Science*, **210**, 115205.

[5] T.G. Myers and F. Font. 2020. Mass transfer from a fluid flowing through a porous media. *International Journal of Heat and Mass Transfer*, **163**, 120374.

[6] T.G. Myers, F. Font and M.G. Hennessy. Mathematical modelling of carbon capture in a packed column by adsorption. 2020. *Applied Energy*, **278**, 115565.

[7] T.G. Myers, A. Valverde and A. Cabrera-Codony. On the development of a consistent mathematical model for adsorption in a packed column (and why standard models fail). Submitted to IJHMT April 2022, `https://papers.ssrn.com/sol3/papers.cfm?abstract_id=4100971`

[8] F. Recasens, B.J. McCoy and J.M. Smith. 1989. Desorption Processes: Supercritical Fluid Regeneration of Activated Carbon. *AIChE Journal*, **35**(6), 951–958.

[9] U.S. Army Chemical Materials Activity. Retrieved June 17, 2022, from `http://www.cma.army.mil/multimediaviewer.aspx?id=943`